Research Square

Preprints are preliminary reports that have not undergone peer review.
They should not be considered conclusive, used to inform clinical practice,
or referenced by the media as validated information.

Hidden Mononuclear Catalysis within Dirhodium(II)/Phosphine Systems: Mechanism, Active Species, and Stereoselectivity

Garima Jindal

gjindal@iisc.ac.in

Indian Institute of Science https://orcid.org/0000-0002-5766-935X

Sapna Rawat

indian institute of science

Debopam Sarkar

Indian Institute of Science

Priyotosh Das

Indian Institute of science

Abhishake Mondal

Indian Institute of Science https://orcid.org/0000-0002-5061-2326

Article

Keywords:

Posted Date: June 17th, 2026

DOI: https://doi.org/10.21203/rs.3.rs-10009400/v1

License: This work is licensed under a Creative Commons Attribution 4.0 International License.
Read Full License

Additional Declarations: There is **NO** Competing Interest.

Hidden Mononuclear Catalysis within Dirhodium(II)/Phosphine Systems: Mechanism, Active Species, and Stereoselectivity

Sapna Rawat,[a] Debopam Sarkar,[b] Priyotosh Das,[a] Abhishake Mondal,[b] and Garima Jindal[a]*

[a]Department of Organic Chemistry, Chemical Sciences Building, Indian Institute of Science, Bengaluru, Karnataka-560012, India

[b]Solid State and Structural Chemistry Unit, Chemical Sciences Building, Indian Institute of Science, Bengaluru, Karnataka-560012, India

email: gjindal@iisc.ac.in

Abstract

Dirhodium(II) carboxylates play a central role in catalysis; nevertheless, achieving high enantioselectivity through the use of external chiral ligands in dirhodium systems has remained elusive until recent years. While these reports using chiral bisphosphines represent landmark breakthroughs, the nature of the active species has not been established, and the proposed coordination modes of phosphines have lacked direct experimental validation. Here, we unambiguously identify the true active catalyst in the dirhodium(II) tetracarboxylate/chiral Josiphos-catalyzed carbonyl arylation reaction. Through a rigorous combination of variable-temperature $^{31}P\{^{1}H\}$ NMR (VT-$^{31}P\{^{1}H\}$ NMR) spectroscopy, electron spray ionization high-resolution mass spectrometry (ESI-HRMS), single-crystal X-ray diffraction (SCXRD), and density functional theory (DFT) calculations, we demonstrate that catalysis proceeds *via* an unprecedented additive-assisted cleavage of the Rh–Rh bond. Under the reaction conditions, the dirhodium(II) core dissociates to form a chiral, orthometalated Rh(III) complex that constitutes the catalytically competent species. This monomeric species demonstrates superior reactivity and stereoselectivity compared to intact dirhodium(II), Rh(I), and alternative Rh(III) complexes, with DFT studies delineating the mechanism and origin of

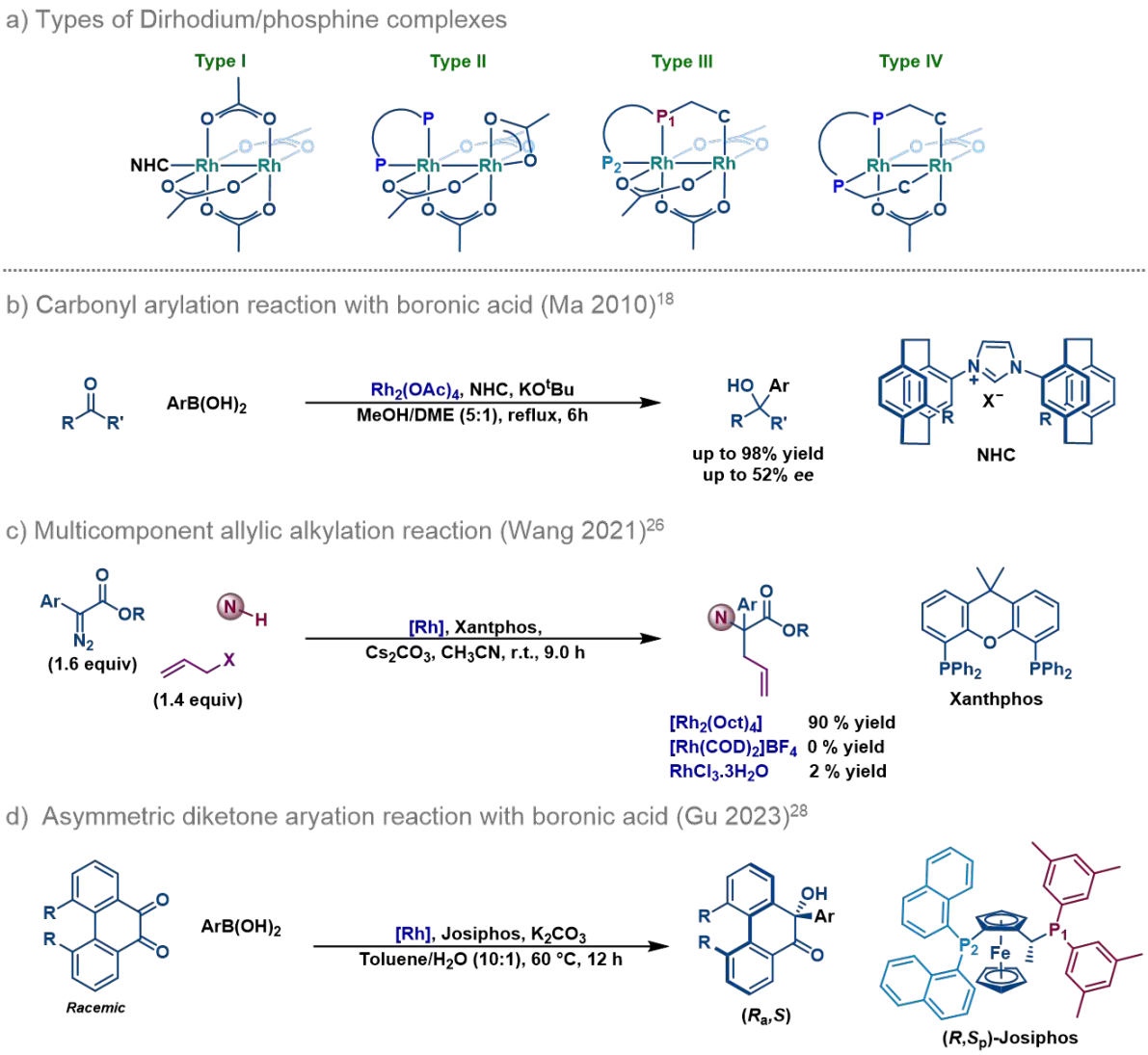
stereocontrol during C–C bond formation. To the best of our knowledge, this work provides the first evidence that dirhodium(II) catalysts — which bear acetate as the bridging ligand and were previously considered resistant to Rh–Rh bond homolysis — can dissociate under catalytic conditions to generate a chiral, orthometalated Rh(III) species as the true active catalyst, prompting a revaluation of dirhodium-catalyzed mechanisms and paving the way for novel asymmetric transformations.

Introduction

Dirhodium(II) tetracarboxylate paddlewheel complexes have found widespread application in homogeneous catalysis owing to their rigid dinuclear frameworks and the presence of accessible axial coordination sites.[1] These complexes are highly efficient catalysts for carbene and nitrene transfer reactions, oxidation processes, and a range of Lewis acid-mediated transformations, often displaying excellent regio-, chemo-, and stereoselectivities.[2–15] The electronic and steric properties of the bridging carboxylate ligands, which link the two rhodium centers, exert a profound influence on both reactivity and stereochemical outcome.[1,16] Consequently, high levels of asymmetric induction are most commonly achieved through the use of chiral bridging carboxylate ligands. This strategy, however, requires the synthesis of discrete, ligand-defined dirhodium complexes prior to catalysis, rendering ligand screening labor-intensive and time-consuming.[1,17] To circumvent these limitations, an alternative approach involves the use of external chiral ligands capable of coordinating to the axial sites of an otherwise achiral dirhodium(II) core; such systems are referred to herein as Type **I** complexes (Scheme 1a). In a seminal contribution, Ma and co-workers demonstrated that coordination of bulky planar-chiral imidazolium salts derived from [2.2]-paracyclophane to an achiral dirhodium(II) complex enabled the arylation of aldehydes with phenylboronic acids with high reactivity but only moderate enantioselectivity (up to 52% *ee*; Scheme 1b).[18] Since that report, only a limited number of studies have explored asymmetric catalysis using Type **I**

dirhodium(II) systems, primarily in carbonyl arylation reactions, typically with modest enantioselectivities and narrow substrate scope.[19–22] The subdued stereocontrol observed in these systems has generally been attributed to the substantial spatial separation between the chiral environment and the reactive metal center, which has in turn curtailed the broader application of dirhodium(II) catalysts in asymmetric transformations. This behaviour stands in marked contrast to many other transition-metal catalytic platforms, wherein simple introduction of an external chiral ligand generates an in situ active species capable of exerting excellent stereochemical control.[23–25]

Recently, Wang and co-workers proposed a new class of dirhodium(II)/bisphosphine complexes, denoted Type **II**, in multicomponent reactions that afford allylic-alkylated products at ambient temperature (Scheme 1c).[26] In these systems, Type **II**, the bisphosphine ligand coordinates at both axial and equatorial positions, giving rise to distinct reactivity patterns relative to Type **I** complexes (Scheme 1a). In principle, the closer proximity of the chiral ligand to the reactive metal center in Type **II** complexes should enable improved stereocontrol. However, only very low *ee*s were achieved with chiral bisphosphine ligands, and no direct experimental evidence was provided to establish Type **II** as the catalytically active species. Subsequent studies demonstrated moderate enantioselectivity (up to 88% *ee*) for indole substrates, indicating a pronounced substrate dependence.[27]

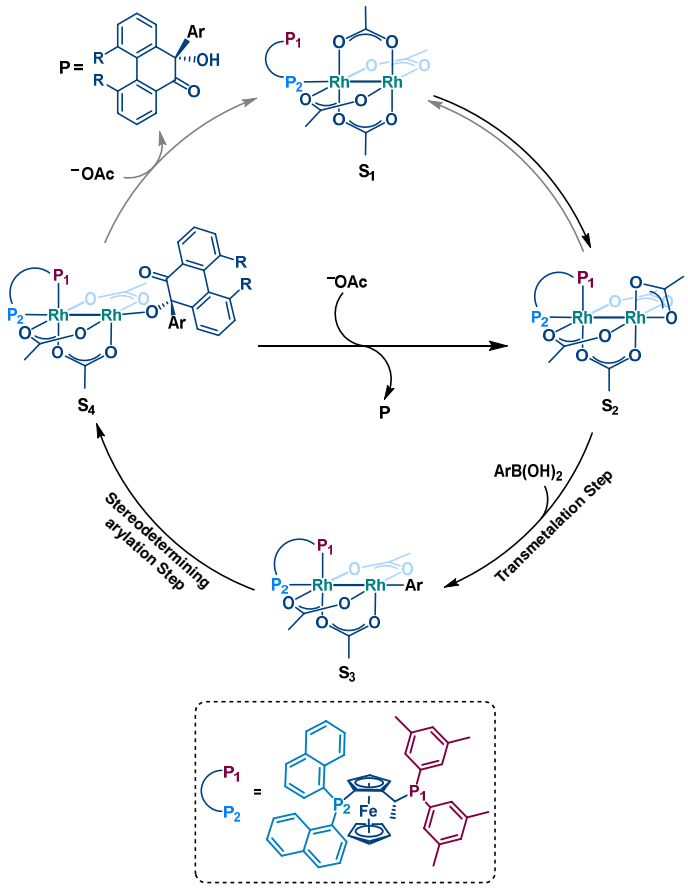


Scheme 1. (a) Types of dirhodium(II)/phosphine complexes and prior reports on dirhodium(II)-catalyzed reactions (b, c, d).

Building on this work, Gu and co-workers reported a highly enantioselective carbonyl arylation reaction employing an achiral dirhodium(II) catalyst in combination with chiral bisphosphine ligands, affording α-hydroxy ketones from racemic substituted phenanthrene-9,10-diones in up to 99 % yield and 96 % *ee* at 60 °C. (Scheme 1d)[28], a platform subsequently extended by the same group to cascades affording quaternary chiral phthalides,[29] asymmetric arylation of

sterically bulky isatins[30] and desymmetrization of bicyclic 1,2-diketones.[31] This study represents the first broadly successful example of enantioselective dirhodium(II)-catalyzed carbonyl arylation and demonstrated the potential of this catalytic platform for extension to other transformations.[28]

Analogous to earlier reports by Wang and coworkers,[26] the active catalyst was proposed to be a Type **II** complex. Although extensive mechanistic investigations—including UV–vis spectroscopy, high-resolution mass spectrometry (HRMS), and kinetic studies—were performed, no direct evidence supporting the formation of a Type **II** species was obtained. Intriguingly, the substitution of the $Rh_2(OAc)_4$ precatalyst with a mononuclear Rh(I)/Josiphos complex or the orthometalated Type **III** species resulted in markedly diminished reactivity and enantioselectivity as shown in Scheme 1d, consistent with the complete inactivity of mononuclear Rh(I) and Rh(III) complexes observed in Wang's system (Scheme 1c). Collectively, these studies highlight the essential role of the intact Rh–Rh framework. Based on their preliminary mechanistic investigations, they proposed a catalytic cycle shown in Scheme 2. The first step involves the conversion of $\mathbf{S_1}$ to the active species $\mathbf{S_2}$. Further, transmetalation with aryl boronic acid generates the complex, $\mathbf{S_3}$, which undergoes stereoselective carbonyl insertion to furnish the arylated product, **P** and simultaneous regeneration of either $\mathbf{S_1/S_2}$.[28] In another related study on β-alkenylation of α, β-unsaturated aldehydes, *ee*s upto 91% were achieved.[32] In addition to Types **I–III**, related Type **IV** complexes (Scheme 1a), in which phosphine ligands bind exclusively in the equatorial plane, have been reported and shown to be competent catalysts in hydro- and dehydrosilylation reactions.[33,34]

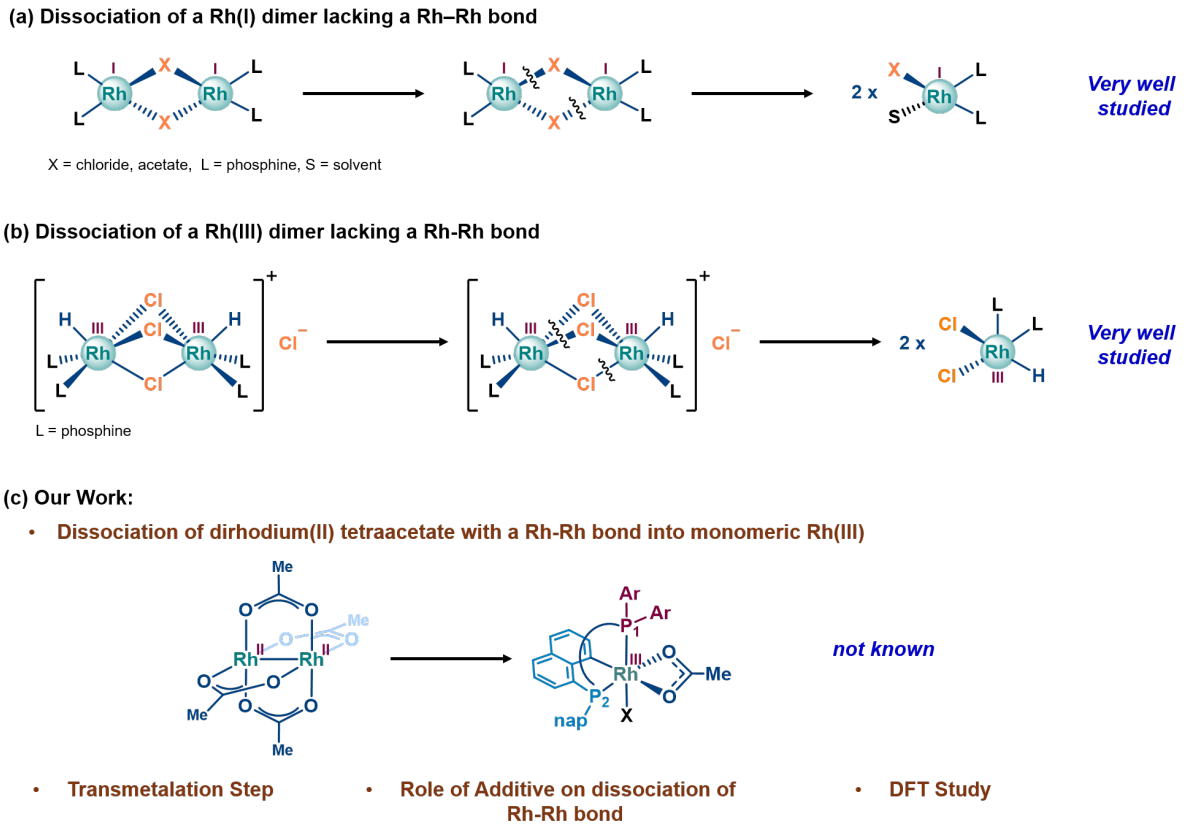


Scheme 2. Proposed catalytic cycle for the dirhodium(II)-catalyzed carbonyl arylation reaction.

Collectively, these studies illustrate how externally added phosphine ligands can adopt multiple coordination modes under different reaction conditions, leading to distinct dirhodium-based species as shown in Scheme 1a. Nevertheless, the identity and role of the putative Type **II** complex remain unresolved, and the origins of the high reactivity and enantioselectivity observed in reactions such as those shown in Schemes 1c and 1d remain unclear. It is important to distinguish the present system from Rh(I) and Rh(III) dimers that lack a Rh–Rh bond and are held together solely by labile bridging ligands (Scheme 3a & 3b).[35,36] Such systems are well established and have been shown to catalyze reactions through monomeric species; they are therefore not directly comparable to the present work (Scheme 3c). Overall, these systems are mechanistically distinct from dirhodium(II) tetracarboxylate complexes, which contain a

formal Rh–Rh single bond. Although Rh–Rh bond dissociation is documented for dirhodium(II) complexes bearing labile triflate bridging ligands,[37-39] this behavior has been explicitly shown not to extend to acetate-bridged dirhodium(II) tetracarboxylates. Furthermore, the dissociated triflate complex has shown to exhibit significantly reduced reactivity, casting shadow on the nature of the true active species. Comparative studies with phosphine donors have demonstrated that acetate coordination blocks equatorial site access and thereby prevents Rh–Rh bond cleavage, in direct contrast to triflate-bridged complexes.[40] Accordingly, the assumption that the intact dinuclear core in dirhodium(II) tetraacetate constitutes the active catalyst has thus persisted by default, rather than by direct experimental verification.

Here we report a comprehensive mechanistic investigation that directly challenges this assumption. As a representative case, we examined the carbonyl arylation reaction reported by Gu and co-workers (Scheme 1d) using an integrated experimental and computational approach.[28] We combine variable-temperature $^{31}P\{^{1}H\}$-NMR (VT-$^{31}P\{^{1}H\}$ NMR) spectroscopy, electrospray ionization high-resolution mass spectrometry (ESI-HRMS), and density functional theory (DFT) calculations together with the synthesis and single-crystal X-ray diffraction (scXRD) to interrogate the exact nature of the catalytically active species. Our results, for the first time, uncover an unexpected transformation under the reaction conditions that leads to the formation of an elusive catalytic species that has not been previously recognized in dirhodium(II) chemistry — one whose identity and mechanistic role fundamentally revise the mechanistic basis of this reaction.



Scheme 3. (a, b) Ligand-lability-driven dissociation of Rh (I) and Rh (III) dimers without Rh–Rh bonds (c) Ligand and additive assisted Rh–Rh bond cleavage revealing the true active species in dirhodium(II) catalysis (this work).

Results and Discussion

We began our investigation by evaluating all plausible coordination modes of the Josiphos ligand to the catalyst dirhodium(II) tetracarboxylate ($Rh_2(OAc)_4$) to identify the most stable species. The possible active species were optimized using the $SMD_{(toluene:water)}$/B3LYP-D3(BJ)/6-311++G(d,p),SDD(Rh,Fe)//B3LYP-D3(BJ)/6-31G(d,p), SDD(Rh, Fe) level of theory in Gaussian 16 software.[41-50] All computational details are given in the supporting information (SI). Our calculations revealed that Type **II** complexes are indeed energetically more stable than species featuring monocoordination of the ligand at the dirhodium(II) core. Among the Type **II** isomers, complex **A9** - in which one of the bridging

carboxylate ligands dissociates resulting in a κ^1 fashion coordination, with a base occupying the axial position is stabilized by 48.5 kcal mol^{-1} relative to **A1**. Since diaxial coordination blocks the reactive site, **A9** is most likely the resting state of the catalyst. The catalytic cycle progresses by dissociation of one of the ligands upon substrate coordination. Interestingly, the orthometalated species, **A7** is also quite stable, however, in the experiments carried out by Gu and coworkers, it exhibited reduced reactivity and selectivity for the reaction shown in Scheme 1d.[28] Thus, we considered detecting/isolating the Type **II** species (**A9** and other related complexes) using various spectroscopic methods as discussed below. A general mechanism of the carbonyl arylation shown in Scheme 2.

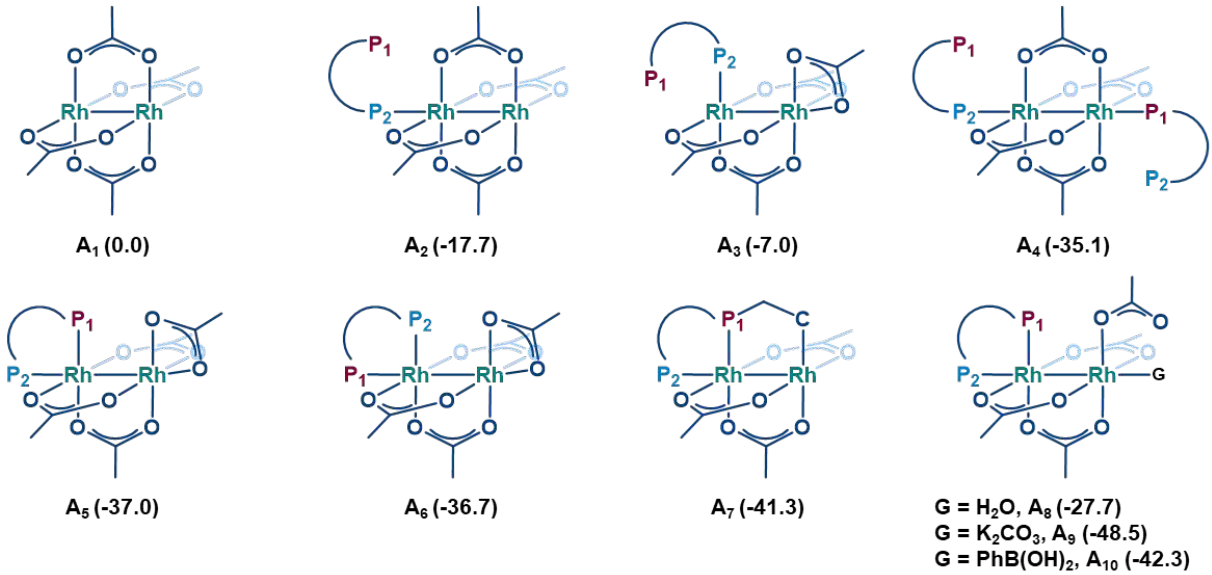


Figure 1. Possible catalytic active species. The relative free energies (kcal mol^{-1}) are given at the SMD$_{(toluene:water)}$/B3LYP-D3(BJ)/6-311++G(d,p),SDD(Rh,Fe)//B3LYP-D3(BJ)/6-31G(d,p), SDD(Rh,Fe) level of theory with relative to **A1**.

Experimental Studies

$^{31}P\{^1H\}$ VT-NMR Spectroscopic Studies

The detection and isolation of active species and reaction intermediates in metal catalysis are inherently challenging and typically require sophisticated mechanistic investigations. In the

present study, $^{31}P\{^{1}H\}$-NMR spectroscopy serves as a particularly powerful tool for probing the coordination modes of phosphine ligands. Owing to its wide chemical-shift window and high sensitivity to changes in the electronic environment, ^{31}P-NMR enables reliable differentiation between distinct phosphorus coordination environments. Seminal studies by Cotton, Chakravarty, Pirano, and Lahuerta have established that $^{31}P\{^{1}H\}$-NMR chemical shifts are highly diagnostic of ligand binding modes in dirhodium(II) complexes.[51-63] In addition, because Rh is NMR-active, Rh-coordinated phosphine species can be readily distinguished from free phosphines or phosphine oxides: the former exhibit characteristic Rh–P coupling patterns (appearing as doublets, doublets of doublets, or related multiplets), whereas the latter typically appear as singlets. In general, phosphorus nuclei coordinated at axial positions resonate upfield, while those bound in equatorial positions resonate downfield, although a limited number of exceptions to this trend have been reported. Representative examples illustrating these characteristic upfield and downfield chemical shifts as a function of phosphine coordination mode with respect to free phosphine ligand are shown in Figure 2.[64.65] Further, a compilation of other known dirhodium(II)/phosphine complexes with their ^{31}P-NMR chemical shifts is provided in the SI (Section 16 of SI). A similar trend was also observed by Gu and coworkers in **M1** and **M2** complexes.[28] The P_1 nuclei of the free chiral Josiphos ligand initially resonated at 6.1 ppm and shifted to -10.1 ppm upon axial coordination in **M1**, whereas, upon equatorial coordination in **M2**, it exhibited resonance at 20.1 ppm. Overall, these observations establish a hallmark for distinguishing the axial versus equatorial coordination of the phosphine ligand in dirhodium(II)/phosphine systems. Furthermore, Type **II** species, if present in the reaction mixture must exhibit resonances close to M_2 (*vide infra*).

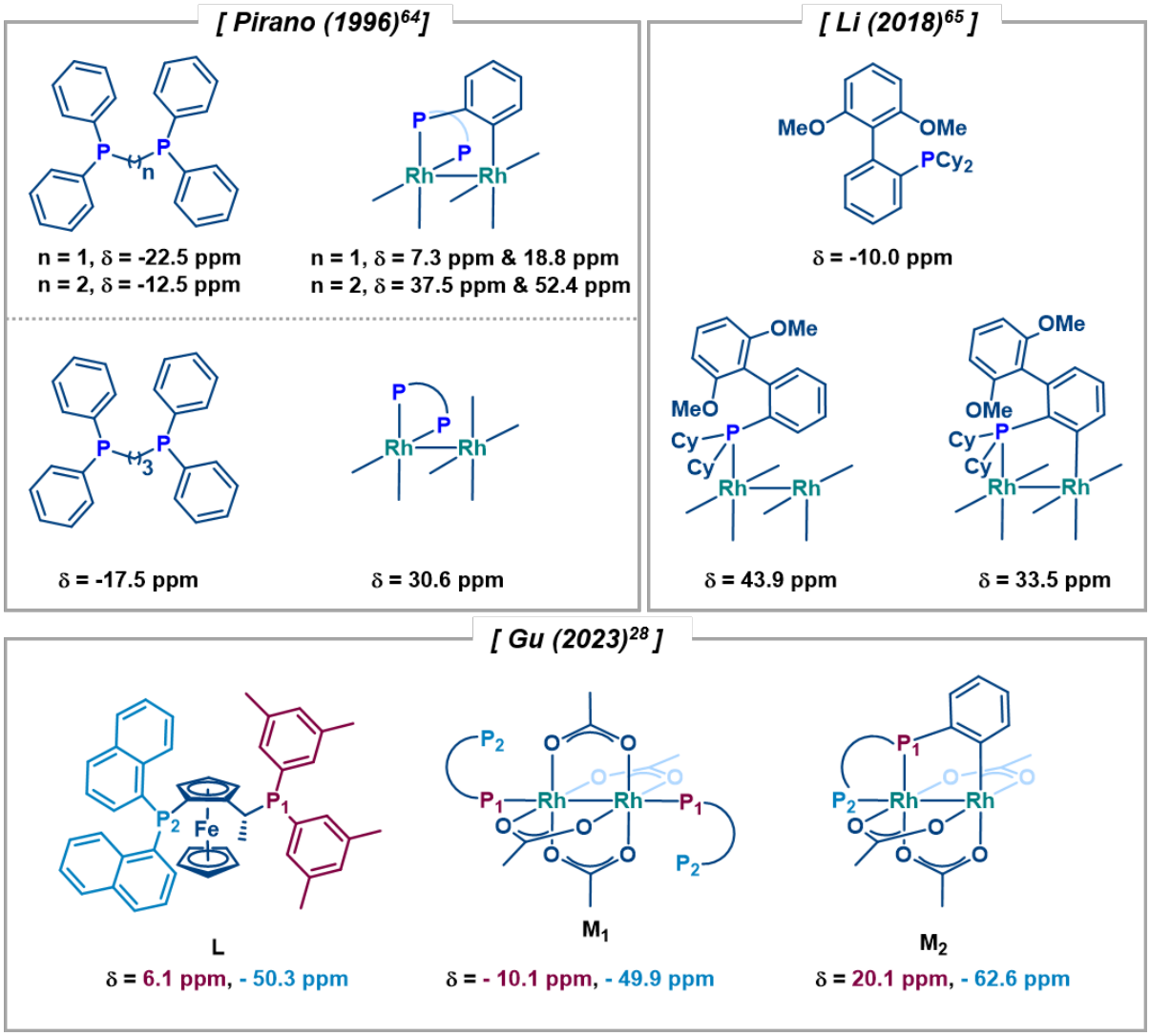


Figure 2. Seminal reports on dirhodium(II)/phosphine complexes with $^{31}P\{^{1}H\}$-NMR chemical shifts.

Thus, we use $^{31}P\{^{1}H\}$-NMR to study ligand coordination dynamics and to identify the active species catalyzing the carbonyl arylation reaction.[28] We begin by taking a 1:2 molar mixture of dirhodium(II) tetraacetate and the chiral Josiphos ligand in toluene, which was monitored over a temperature range from room temperature to 80 ºC as shown in Figure 3. At 40 ºC, the spectrum was dominated by intense signals corresponding to the free Josiphos ligand, with P_1 and P_2 nuclei resonating at 6.1 ppm and -50.3 ppm, respectively. After 2.5 h at 60 ºC, two new intense signals appear at 62.8 ppm (doublet), together with a signal at -41.6 ppm (singlet).

Based on the axial–equatorial coordination trends of phosphine ligands as discussed above, these resonances may correspond to a species in which the P_1 nucleus is equatorially coordinated to Rh, while the P_2 nucleus remains uncoordinated, as indicated by its proximity to the chemical shift of free P_2 as shown in Figure 3. Upon further heating, new signals, mainly doublets of doublets (dd) and doublet, appear in the downfield or positive region, indicating the coordination of Josiphos ligand to the Rh atom. Several pairs of dd signals (highlighted in the same colour) shared a common second coupling constant, consistent with a P–Rh–P arrangement in which two chemically inequivalent phosphorus nuclei are coupled via the same Rh atom (Figure 3). In our spectra, we do not observe any dd signals in upfield or negative region, unlike the **M_2** complex. A Type **II** species if present must resonate at similar chemical shifts. While it is difficult to assign a structure based on the spectra in Figure 3 alone, it is clear that there is no complex containing an axially coordinated phosphine to Rh metal.

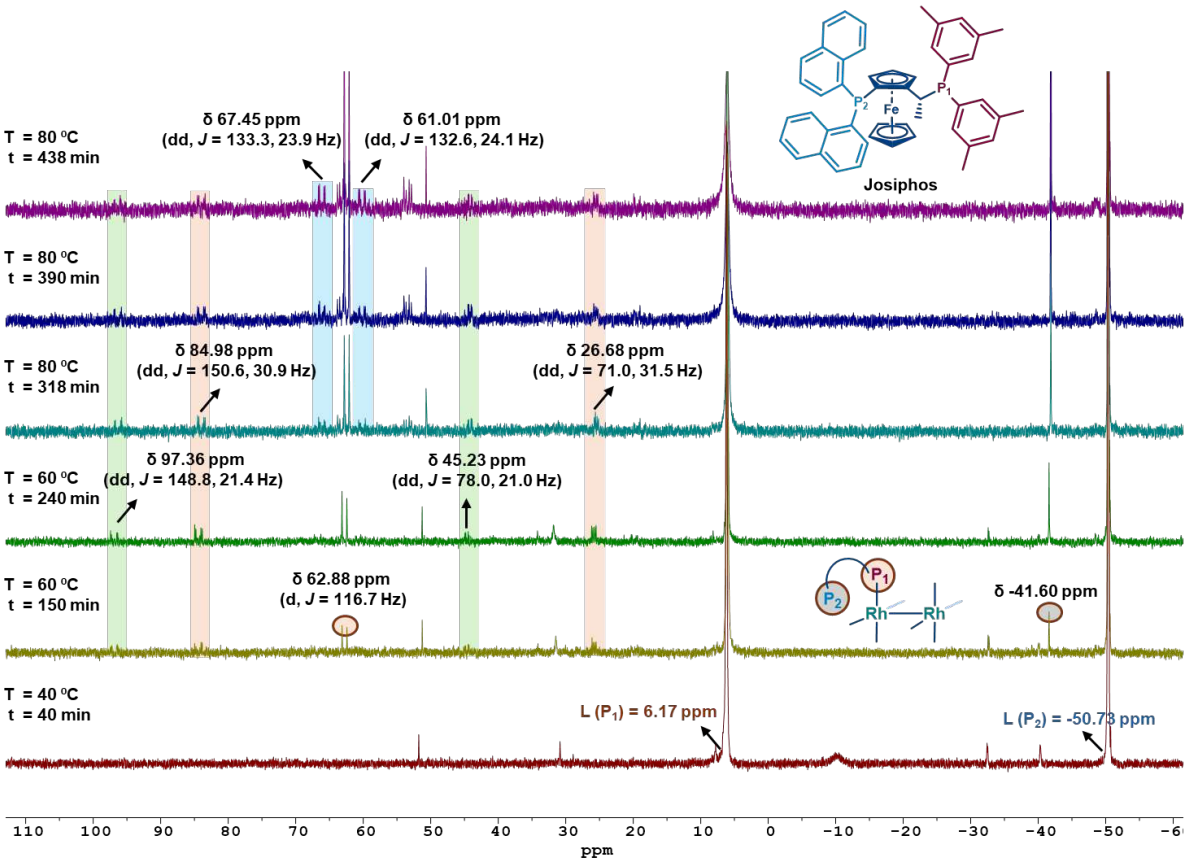


Figure 3. Stack plots of variable-temperature (25–80ºC) $^{31}P\{^{1}H\}$-NMR of $Rh(OAc)_4$/Josiphos mixture. Conditions: $Rh_2(OAc)_4$ (0.025 mmol, 1.0 equiv) and Josiphos (0.05 mmol, 2.0 equiv) were mixed in 0.75 mL of toluene and then transferred to an NMR tube for the analysis.

We next carried out a second $^{31}P\{^{1}H\}$ VT-NMR experiment to monitor a reaction as shown in Scheme 1d in the presence of phenylboronic acid, base and water along with $Rh_2(OAc)_4$ and Josiphos, but without substrate (Figure 3). Because transmetalation is expected to occur under these conditions, leading to the formation of a Rh–Ph species, at least one of the doublet of doublets (dd) signals observed in Figure 3 should exhibit a chemical-shift change. Such changes would aid in identifying the $^{31}P\{^{1}H\}$-NMR signatures associated with the catalytically active species. A careful comparison of the resulting $^{31}P\{^{1}H\}$ VT-NMR spectrum (Figure 4a) with the spectrum obtained in the absence of phenylboronic acid (Figure 3) revealed two key observations: (1) the appearance of new resonances at 44.82 ppm and 65.25 ppm, highlighted in pink and hereafter denoted as $\mathbf{X_2}$; and (2) the disappearance of resonances at 61.0 ppm and 67.4 ppm, highlighted in blue in Figure 3 and hereafter assigned to $\mathbf{X_1}$. The structural identity of $\mathbf{X_1}$ will be discussed in detail below (*vide infra*). Notably, all other dd signals remained unchanged. In addition, some signals (highlighted in grey) were observed that were also detected during independent $^{31}P\{^{1}H\}$-NMR monitoring of a Rh(I) complex (Figure S8 in SI). These resonances are therefore most plausibly attributed to a monorhodium(I) species as shown in Figure 4a. However, monorhodium(I) complexes delivered substantially reactivity and moderate enantioselectivity as shown in Scheme 1d.[28] Taken together, these observations strongly suggest that $\mathbf{X_1}$ serves as a precursor to the transmetalated complex, $\mathbf{X_2}$ and represents the most likely catalytically active species in the reaction.

It is worth mentioning here that Gu and coworkers also reported a ^{31}P-NMR spectrum of the reaction mixture, exhibiting two dominant peaks at 44.4 ppm and 64.9 ppm (similar to $\mathbf{X_2}$), which were also proposed to correspond to the transmetalated complex as shown in Figure

4c.[28] However, the structure proposed is a Type **II** species with the P_2 nuclei in an axial position and the P_1 nuclei in an equatorial position. Based on our above discussion, it is unlikely that Type **II** complex will exhibit resonances in the positive region alone.

Thus far, although we have been able to identify the $^{31}P\{^1H\}$-NMR signals corresponding to the most likely catalytically active species, $\mathbf{X_1}$ and its subsequent transmetalated complex, $\mathbf{X_2}$, the precise structures of these species remained unknown. The observed chemical-shift values suggest either a species in which both $\mathbf{P_1}$ and $\mathbf{P_2}$ are equatorially coordinated to a dirhodium core, or alternatively, a mononuclear Rh(I)/Rh(III) complex (Figure 4b). To distinguish between these possibilities and to enable definitive structural assignment, we therefore pursued the synthesis and isolation of $\mathbf{X_1}$ complex, guided by prior reports describing the preparation of equatorially coordinated dirhodium(II)/phosphine complexes.[52,54,55,57,58]

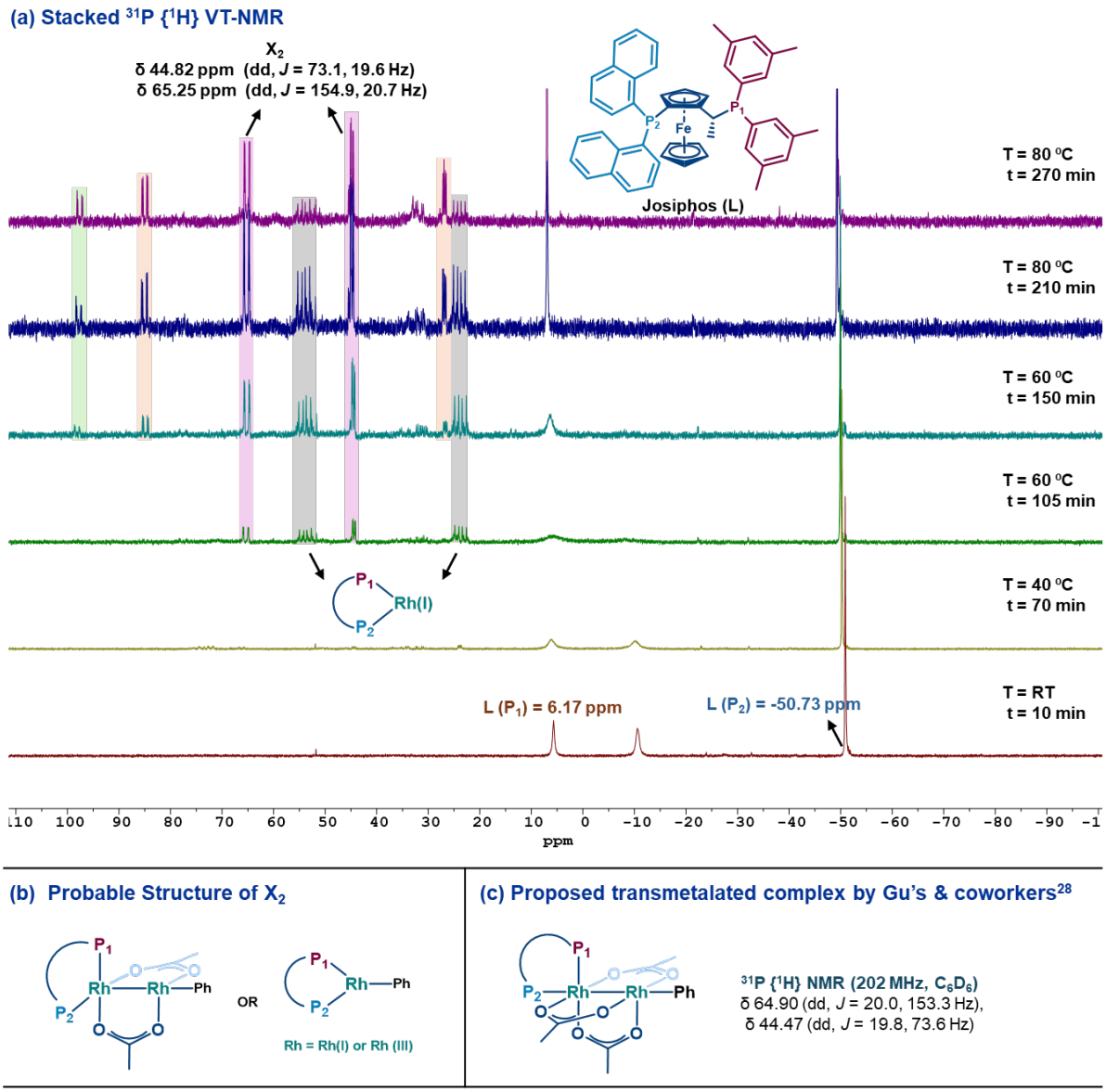


Figure 4. (a) Control experiment highlighting the formation of proposed transmetalated complex, monitored by $^{31}P\{^{1}H\}$ VT-NMR. Conditions: $Rh_2(OAc)_2$ (0.025 mmol, 25 mol %), Josiphos (0.050 mmol, 50 mol%), $PhB(OH)_2$ (0.25 mmol, 2.5 equiv) and K_2CO_3 (0.10 mmol, 1equiv) were mixed in toluene (0.75 mL) and H_2O (75 µL), then transferred to an NMR tube for the analysis. (b) Probable structure of **X₂** complex. (c) Transmetalated complex proposed by Gu and coworkers.[28]

Synthesis and Characterization of X₁ Complex

A 1:1 mixture of commercially purchased TCI dirhodium(II) tetraacetate ($Rh_2(OAc)_4$) and Josiphos with 2.0 equivalent of KCl was heated in anhydrous toluene and acetic acid (10:2, v/v) under an inert atmosphere at 80 ºC for 3.5 h (Scheme 4a). The rationale for the addition of KCl is discussed below. The reaction mixture was subjected to $^{31}P\{^1H\}$-NMR, and similar dd signals seen in Figure 3 were observed here, too. The resulting orange solid, **X_1**, was isolated, purified, and fully characterized by $^{31}P\{^1H\}$ and ^1H-NMR, and ESI-HRMS. Red block crystals suitable for scXRD were obtained via slow vapor diffusion of n-pentane into a saturated toluene solution of the complex. According to the crystallographic analysis at 150 K, the complex crystallizes in the Monoclinic *P* 2_1 space group. There are two molecules per unit cell (Z=2) with one solvent molecule toluene with each complex. (Table S2 in SI) From the structural perspective, **X_1** is a C–H metalated mononuclear Rh(III) complex, in which the rhodium center is coordinated to two phosphorus atoms, one carbon atom of the naphthalene ring of ligand L, and one acetate ligand bound in a bidentate fashion through two oxygen atoms along with one chloride at sixth coordination site (Scheme 4a). This supports the existence of rhodium as Rh(III) in the complex. The coordination geometry is distorted octahedral as confirmed from the SHAPE calculations. (Table S4 in SI) This can also be visualized from the difference in bond angles among the equatorial donor atoms (∠O1-Rh1-O2= 59.7º, ∠P1-Rh1-C17= 84.05º, ∠C17-Rh1-O1= 101.96º, ∠O2-Rh1-P1= 114.01º). There is presence of multiple intra- and intermolecular H-bonding interactions with terminal Cl atom and O atoms from acetate which stabilizes the structure. DFT calculations further supported this structural assignment, with the optimized geometry showing excellent agreement with the experimentally determined crystal structure (Scheme 4b). ESI-HRMS data of **X_1** complexes were recorded and showed dominant peaks at m/z = 899.1376 corresponding to a monorhodium complex.

Initial attempts to synthesize **X_1** were carried out using BLD Pharma $Rh_2(OAc)_4$ and Josiphos without any added chloride source, which afforded **X_1** in sufficient quantity for characterization

including ScXRD. However, the yield of **X1** was varying across different purchased batches of BLD Pharma $Rh_2(OAc)_4$. ScXRD data revealed that the electron density map at the sixth coordination site was best modeled as a chloride ligand, despite the absence of any chlorine-containing reagents in the synthesis. To confirm this assignment, ^{35}Cl NMR spectroscopy of the isolated **X1** complex was performed, which confirmed the presence of chloride with a resonance at 34.7 ppm (Figure S5 in SI). This unexpected finding prompted us to investigate the origin of the chloride ligand.

As the starting material for the synthesis of $Rh_2(OAc)_4$ is rhodium(III) chloride, $RhCl_3$, we considered the possibility that chloride as an impurity could remain in the commercially available dirhodium(II) source and be incorporated into the **X1** complex. To verify this, we initially attempted to synthesize the **X1** complex using a different commercially available $Rh_2(OAc)_4$ from Sigma-Aldrich and TCI Chemicals without any added chloride source. However, no $^{31}P\{^1H\}$-NMR signals corresponding to the **X1** complex were observed, whereas addition of KCl to the TCI $Rh_2(OAc)_4$ reaction mixture afforded **X1** cleanly.

From our detailed mechanistic investigations (*vide infra*), we established that phenylboronic acid and water play a crucial role in driving the formation of the **X1** complex. Based on this insight, we designed three control experiments to further validate the source of chlorine and to probe the identity of active monorhodium(III) species forming with TCI $Rh_2(OAc)_4$:

(1) TCI $Rh_2(OAc)_4$ alone,

(2) TCI $Rh_2(OAc)_4$ with added KCl, and

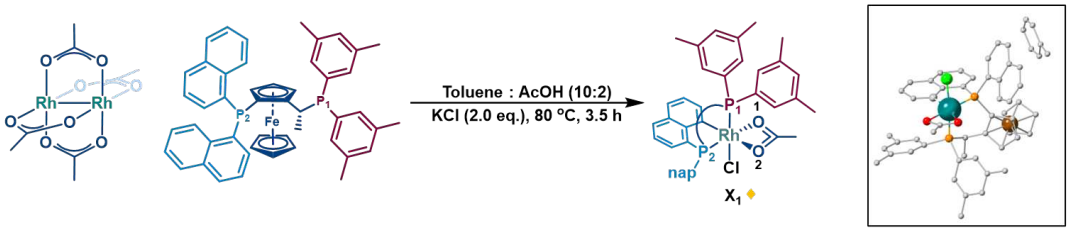
(3) BLD Pharma $Rh_2(OAc)_4$

Comparison of the $^{31}P\{^1H\}$-NMR spectra revealed that, in the presence of KCl, signals corresponding to the **X1** complex (yellow diamond), were clearly detected with TCI $Rh_2(OAc)_4$ (Scheme 4c). In contrast, in the absence of KCl, two new resonances appeared at 57.63 and

62.54 ppm (red diamond), in the 50–65 ppm region (Scheme 4c). These signals were never observed in any experiments conducted with BLD $Rh_2(OAc)_4$. Notably, these signals were absent in the $^{31}P\{^1H\}$ VT-NMR spectrum obtained using TCI $Rh_2(OAc)_4$ in the presence of phenylboronic acid (Section 5.2, SI), and new signals corresponding to the transmetalated complex were observed (*vide infra*). Collectively, these observations indicate that the resonances at 57.63 and 62.54 ppm most likely correspond to an active monorhodium(III) species bearing a different ligand instead of chloride or a cationic complex with a counter anion, and chloride incorporation in the $\mathbf{X_1}$ complex most likely originates from the chloride impurity retained in the commercially sourced dirhodium(II) precursor.

It is important to note that the while the presence of chloride facilitates crystallization, the identity of this ligand—chloride or otherwise—has no impact on the reactivity or enantioselectivity of the catalyst, as all commercially available dirhodium(II) precursors furnished similar yields and *ee* values (Table S1, entry 11). We would also like to highlight here that irrespective of the source of the dirhodium precursor, the transmetalated species remains similar.

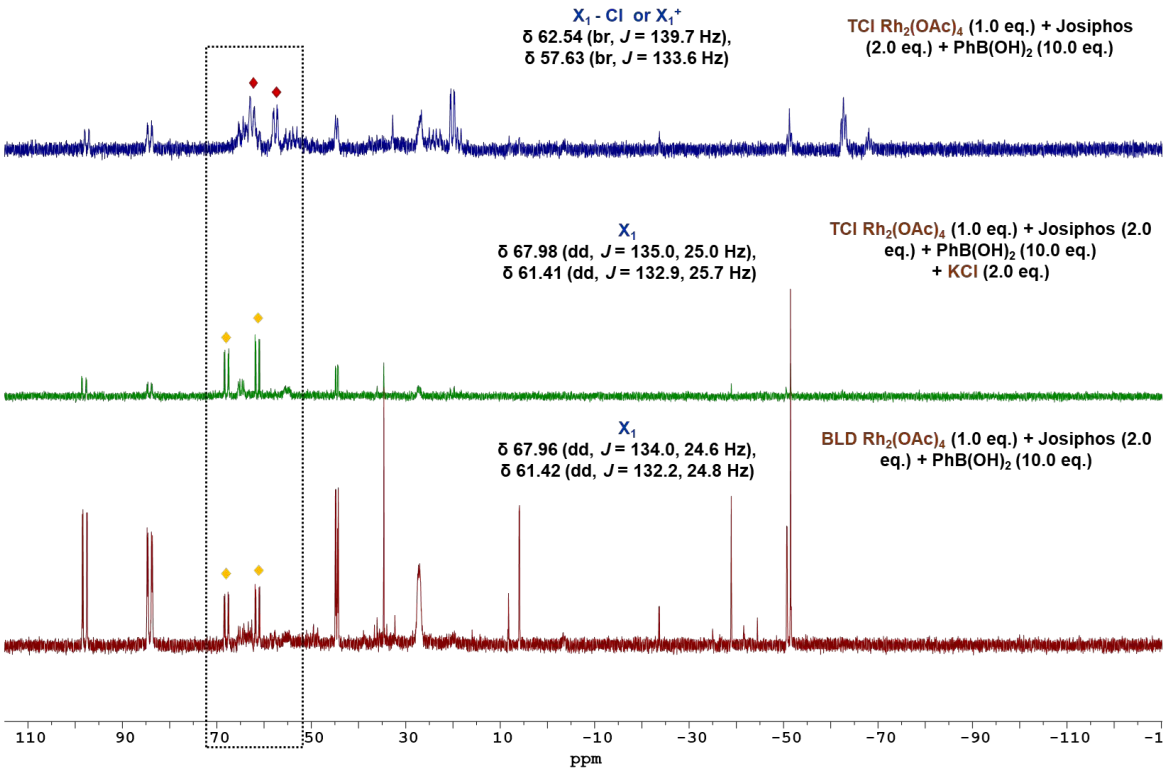
(a) Synthesis of C-H metalated monorhodium(III)/Josiphos complex



(b) Structural parameters comparison of X_1

Parameters	Rh-P_1	Rh-P_2	Rh-O1	Rh-O2	Rh-Cl	Rh-C	∠Cl-Rh-P_1	∠O1-Rh-P_2	∠O2-Rh-C
Crystal structure	2.28	2.27	2.18	2.25	2.35	2.01	173.73	172.51	161.66
Optimized geometry	2.25	2.31	2.19	2.27	2.38	2.00	174.64	171.78	163.02

(c) Stacked $^{31}P\{^1H\}$-NMR Spectra Revealing the Origin of Chloride in the X_1



Scheme 4. (a) Synthesis of **X1** complex. (b) Structural parameter comparison of **X1** complex. **(c)** Stack plots of $^{31}P\{^1H\}$-NMR of reaction monitored over 4 h to detect the source of chlorine atom.

Transmetalation Step

To definitively establish the identity of the $\mathbf{X_2}$ species observed in Figure 3, $\mathbf{X_1}$ was subjected to transmetalation conditions. Treatment of $\mathbf{X_1}$ with $PhB(OH)_2$ (2.0 equiv) and K_2CO_3 (2.0 equiv) in toluene (0.8 mL)/H_2O (80 μL) at room temperature led to rapid and clean spectral changes, as monitored by $^{31}P\{^1H\}$-NMR spectroscopy. Within 10 min, the dd signals at δ 61.42 and 68.54 ppm (yellow diamond), assigned to X_1, disappeared completely. Concomitantly, a new pair of dd signals at δ 44.31 and 65.80 ppm (green diamond) emerged, corresponding to $\mathbf{X_2}$ (Figure 5). No additional phosphorus-containing species were detected, consistent with a direct transmetalation event at the rhodium center. Furthermore, comparison with the $^{31}P\{^1H\}$-NMR spectra in Figures 3 and 4a confirms that only the signals at δ 61.42 and 68.54 ppm are perturbed upon addition of phenylboronic acid, while resonances in the more deshielded region remain unchanged, demonstrating that other species — whether dirhodium or monorhodium — are not involved in this transformation.

ESI-HRMS analysis of $\mathbf{X_2}$ revealed a dominant peak at m/z 917.1806, consistent with a monorhodium(III) transmetalated complex. Collectively, these data unambiguously confirm that the resonances at δ 44.31 and 65.80 ppm arise from the transmetalated species $\mathbf{X_2}$.

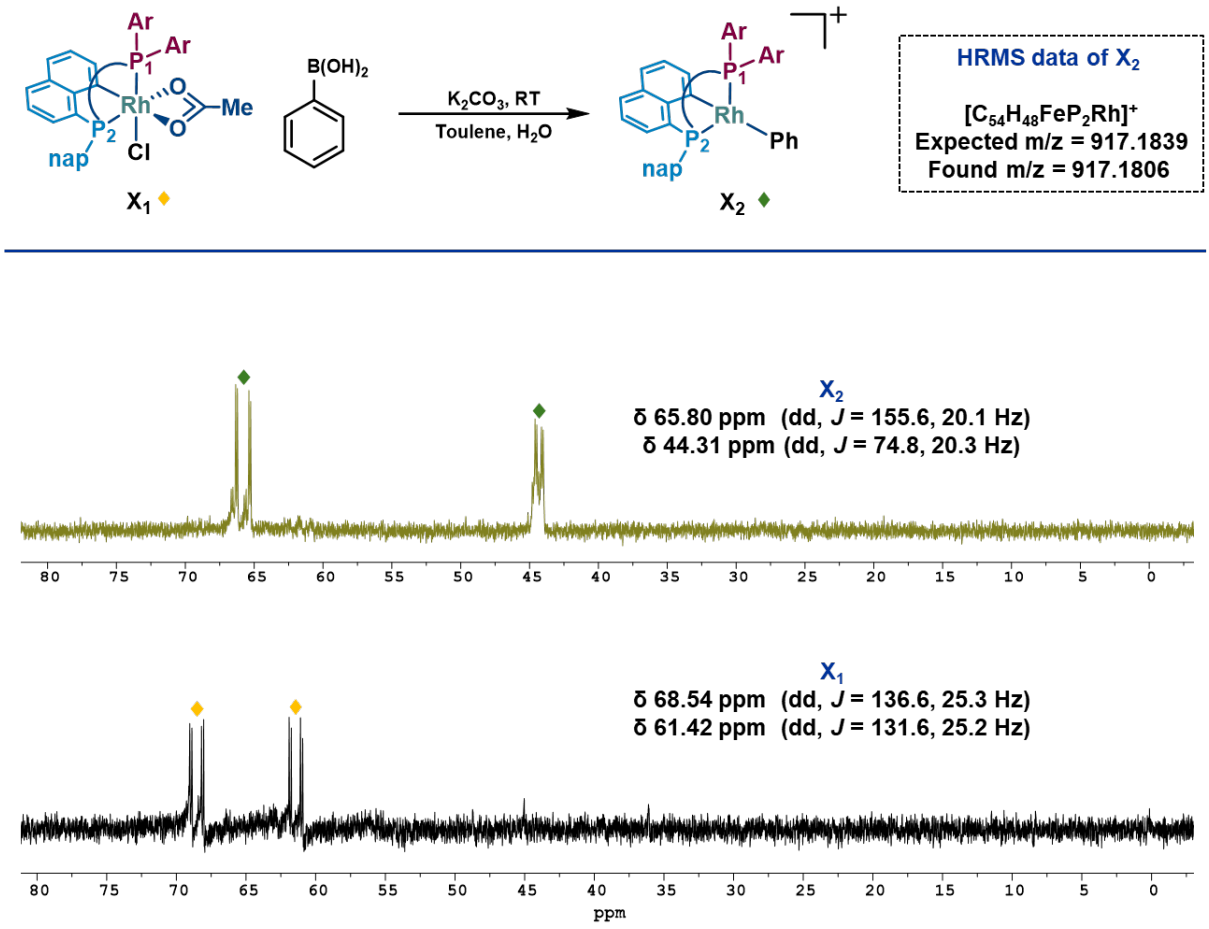


Figure 5. Control experiment demonstrating the transmetalation of $\mathbf{X_1}$ to $\mathbf{X_2}$, monitored by $^{31}P\{^1H\}$-NMR and ESI-HRMS spectrometry.

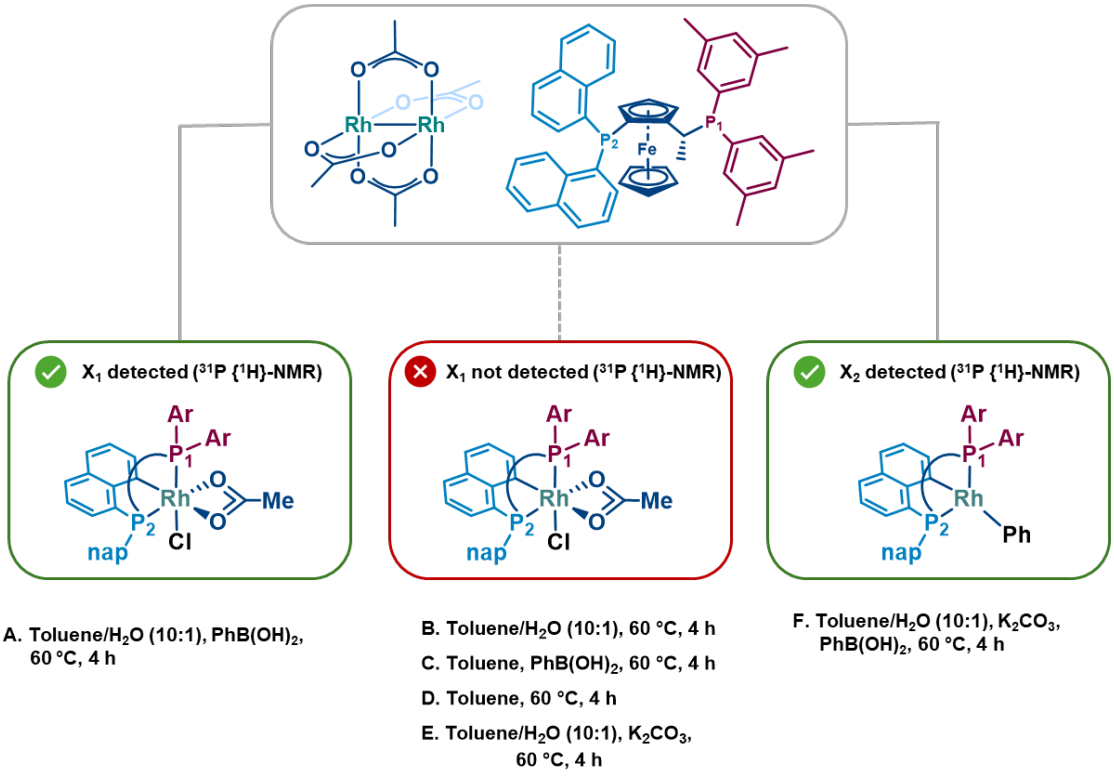
Together with the scXRD analysis of $\mathbf{X_1}$, our results demonstrate that $\mathbf{X_1}$ and $\mathbf{X_2}$ are ortho-metalated monorhodium(III) complexes rather than dirhodium(II) complexes. As discussed above, while the dissociation of triflate complex is known, the dissociation of the Rh–Rh bond has not been reported for with acetate as the bridging ligand. We would like to add here that the dissociation of Rh(I) dimers in the presence of solvents/ligands is quite common in literature and differs from the dirhodium (II) work discussed here. We next discuss the factors governing this dissociation under the actual reaction conditions.

Factors Governing Rh–Rh Bond Dissociation

Further inspection of the $^{31}P\{H\}$ VT-NMR spectra (Figures 3 and 4a) revealed a pronounced additive effect on the speciation kinetics. In the absence of additives, the diagnostic resonances assigned to $\mathbf{X_1}$ emerge only after ~5 h (Figure 3), whereas in the presence of phenylboronic acid, base, and water the spectrum is instead dominated by the characteristic signals of $\mathbf{X_2}$ within ~2.5 h (Figure 4). Because $\mathbf{X_1}$ is the precursor to $\mathbf{X_2}$, these observations imply that the additives accelerate formation of $\mathbf{X_1}$. This, in turn, raises a key mechanistic question: is the rate enhancement distributed across all additives, or is it driven primarily by a single component or a specific additive combination?

For a direct comparison, we performed a series of additive-controlled experiments over a 4 h period (Scheme 5). These studies revealed that the combination of phenylboronic acid and water (condition A) is primarily responsible for promoting Rh–Rh bond cleavage to generate $\mathbf{X_1}$, whereas the base plays a crucial role in the rapid conversion of $\mathbf{X_1}$ into $\mathbf{X_2}$ (condition F). In contrast, Gu and co-workers reported first-order kinetics with respect to phenylboronic acid, the dirhodium(II) catalyst, and the ligand, and consequently proposed transmetalation as the rate-determining step.[28] Our results, however, point to a different mechanistic scenario. Because phenylboronic acid and water significantly accelerate Rh–Rh bond dissociation at 60 ºC, leading to the formation of $\mathbf{X_1}$ within ~2.5 h, the previously observed kinetic dependence on phenylboronic acid is more plausibly attributed to its involvement in generating $\mathbf{X_1}$ rather than in the subsequent transmetalation step. Consistent with this interpretation, once $\mathbf{X_1}$ is formed, transmetalation proceeds rapidly, occurring within approximately 10 minutes at room temperature. Collectively, these observations indicate that cleavage of the dirhodium(II) core to form the catalytically competent monorhodium(III) species is the most likely rate-determining step of the catalytic cycle. These findings further underscore the dual role of phenylboronic acid in both facilitating Rh–Rh bond dissociation and enabling efficient

downstream reactivity. While our experiments clearly establish that the dirhodium(II) core dissociates to form a chiral orthometalated monorhodium (III) species, the detailed mechanism underlying this transformation remains unclear and will require a further comprehensive computational and experimental investigation, which will be reported in due course.



Scheme 5. Control experiments to delineate the role of additives in dirhodium(II) dissociation.

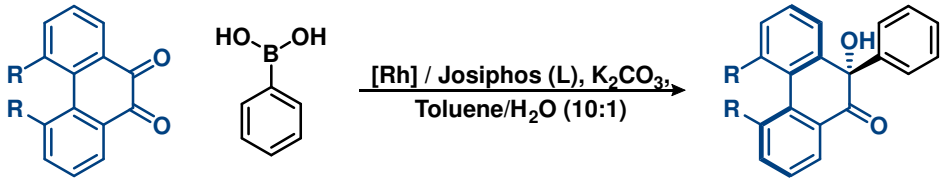
Catalytic Activity of X_1 Complex

After elucidating key mechanistic features—including the transmetalation step and the role of phenylboronic acid and water in promoting Rh–Rh bond cleavage—we next evaluated the catalytic performance of complex **X1**. For substrate 1a (R = Me), the dirhodium(II)/Josiphos system reported by Gu and co-workers delivered the arylated product in high yield and excellent enantioselectivity (up to 96% *ee*; Table 1, entry 1).[28] In contrast, the corresponding monorhodium(I)/Josiphos complex exhibited low reactivity with moderate *ee* (Table 1, entry 2).[28] Remarkably, use of 2.5 mol% of the isolated **X1** complex resulted in complete

conversion within 6 h, affording the product in excellent yield and *ee* (Table 1, entry 3), whereas the standard dirhodium(II)/Josiphos protocol required 12 h to reach a comparable level of conversion. These observations are fully consistent with formation of $\mathbf{X_1}$ being the rate-determining step of the catalytic cycle; once generated, $\mathbf{X_1}$ rapidly catalyzes the transformation, establishing it as the true active species.

To further probe the scope of this catalyst, we examined the enantioselective arylation of phenanthrene-9,10-dione, **1b**, a transformation that has not been previously reported with good enantioselectivity. Under identical conditions, the dirhodium(II)/Josiphos system furnished the desired product in high yield but with very low *ee* (Table 1, entry 5). In striking contrast, the $\mathbf{X_1}$ complex afforded complete conversion within 20 min, delivering the product in excellent yield and high *ee* (Table 1, entry 4). Other monorhodium complexes were also evaluated under the same conditions (Table 1, entries 6 &7) showed no appreciable *ee*, highlighting $\mathbf{X_1}$ as a uniquely effective catalyst for this transformation. A comparison of entries 1 and 5 warrants a discussion. The lower selectivity in the case of substrate **1b** is possibly due to its faster reactivity. Before the complete conversion of dirhodium to $\mathbf{X_1}$, the reaction is being catalyzed by a dirhodium(II) species itself, which results in good reactivity but poor selectivity. To rationalize this superior reactivity and stereocontrol, we next carried out a detailed DFT investigation of the catalytic pathway involving the $\mathbf{X_1}$ complex.

Table 1. Comparative catalytic evaluation of $\mathbf{X_1}$ and other Rh catalysts



1
1a (R = Me)
1b (R = H)

2

3
3a (R =Me)
3b (R= H)

entry	[Rh]	Josiphos	Temperature	Time	Yield/*ee* of 3 (in %)
1	$Rh_2(OAc)_4$ (2.5 mol%)	5.0 mol%	60 ºC	12 h	99/*96*
2	$[Rh(C_2H_4)Cl]_2$ (2.5 mol%)	5.0 mol%	60 ºC	-	56/*85*
3[a]	X_1 (2.5 mol%)	-	60 ºC	6 h	94/*99*
4[b]	X_1 (2.5 mol%)	-	60 ºC	20 min	95/*91*
5[c]	$Rh_2(OAc)_4$ (2.5 mol%)	5.0 mol%	60 ºC	8 h	97/*10*
6[c]	$[Rh(C_2H_4)Cl]_2$ (2.5 mol%)	5.0 mol%	60 ºC	8 h	97/-
7[c]	$RhCl_3$ (2.5 mol%)	5.0 mol%	60 ºC	8 h	97/-

Entries 1& 2 were taken from Gu' s work[28], where **1** is **1a**. [a]Conditions: **1a** (0.4 mmol), **2** (1.0 mmol), K_2CO_3 (0.40 mmol), Toluene (3.0 mL) and H_2O (0.3mL). [b]Conditions: **1b** (R = H, 0.1 mmol), **2** (0.9 mmol), K_2CO_3 (0.1 mmol), Toluene (0.8 mL), H_2O (80 µL). [c]Conditions: **1b** (0.3 mmol), **2** (0.75 mmol), K_2CO_3 (0.3 mmol), Toluene (2.0 mL), H_2O (0.2 mL). n.d. (not detected).

DFT Studies

DFT calculations were carried out to construct a catalytic mechanism consistent with the experimental observations described above. All calculations were performed using the phenanthrene-9,10-dione substrate. As discussed above, the **X1** complex, with or without a chloride ligand, yields the same transmetalated complex. Therefore, we initiated our calculations by considering the cationic **B** species as the starting complex, also detected by mass spectrometry, with the vacant sixth coordination site at Rh vacant (Figure 6a). All stationary points were optimized using the $SMD_{(toluene:water)}$/B3LYP-D3(BJ)/6-311++G(d,p),SDD(Rh,Fe)//B3LYP-D3(BJ)/6-31G(d,p), SDD(Rh,Fe) level of theory. Additional calculations at a different basis set and functional are given in the SI (Table S9, S10).

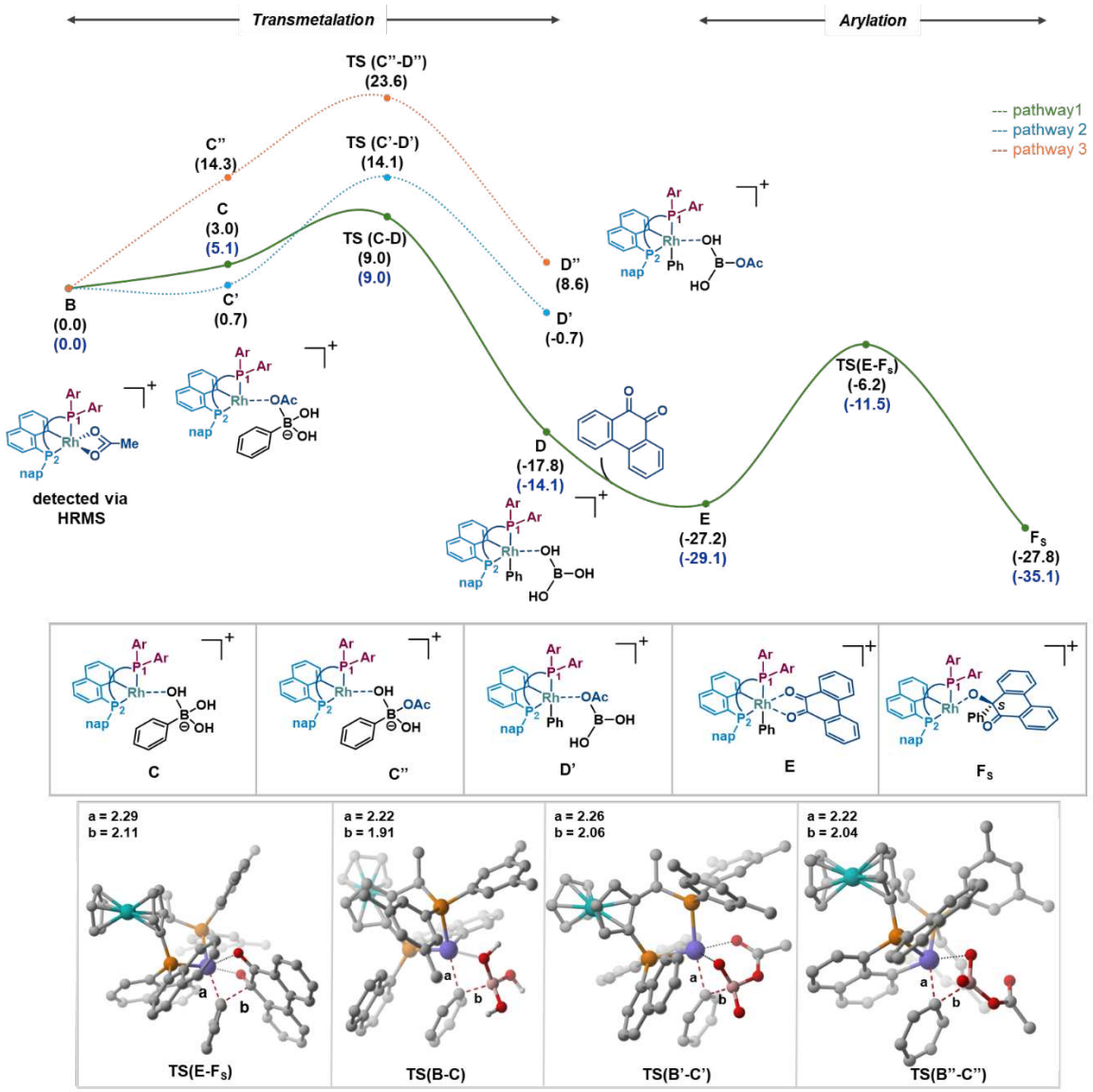
In 2021, Paton, Fletcher and co-workers investigated the mechanism of the Rh(I)-catalyzed Suzuki–Miyaura coupling reaction and reported that formation of a Rh–OH intermediate was a prerequisite for the transmetalation step.[66] In contrast, our experimental studies showed that

the combined addition of $PhB(OH)_2$, K_2CO_3, and H_2O to the **X_1** complex furnished the transmetalated complex, **X_2**, immediately, as confirmed by $^{31}P\{^1H\}$ NMR and ESI-HRMS, with no evidence for the formation of a Rh–OH intermediate. On this basis, three plausible transmetalation pathways were considered, differing in the nature of the activated phenylboronic species: (1) via $[PhB(OH)_3]^-$, assuming K_2CO_3 and H_2O activating the $PhB(OH)_2$ by OH^- group (2) via $[PhB(OH)_2(OAc)]^-$ with acetate group coordinated to Rh, activation of $PhB(OH)_2$ via OAc^- group coordinated to Rh and (3) via $[PhB(OH)_2(OAc)]^-$ with hydroxide coordinated to Rh, activation of $PhB(OH)_2$ via external OAc^- group (Figure 6a). Among these pathways, the $[PhB(OH)_3]^-$ mediated route exhibited the lowest activation free energy barrier ($\Delta G^{\ddagger}$ = 9.0 kcal mol^{-1}) via transition state **TS(C–D)**.

Subsequently, all possible substrate-bound intermediates were evaluated, considering coordination of potential ligands such as acetic acid, acetate, water, and boronic acid (Figure S24 of SI). Among these, complex **E** was found to be the most stable, in which both carbonyl groups of the substrate are coordinated to the Rh atom, with no ligand coordination. We then focused on the stereo-determining arylation step. All plausible diastereomeric transition states (TSs) were evaluated (Figure S25 of SI), and the pathway where only substrate is coordinated to Rh(III) was found to have the lowest activation barrier (Figure 6a). Nucleophilic attack of the phenyl group at the carbonyl carbon can occur from either the *re* or *si* face, leading to the formation of the *S* and *R* enantiomeric product, respectively, in which the arylated product remains coordinated to the Rh centre through an oxygen atom. Subsequent protonation releases the final product. Importantly, extensive conformational sampling was performed for the diastereomeric transition states to confirm the lowest-energy transition states (Section 16 in SI). Further, to get better estimate of the energy difference between the lowest diastereomeric TSs, DLPNO-CCSD(T) calculations were carried out and the difference in free energy between the competing diastereomeric transition states was found to be 4.3 kcal/mol, corresponding to

99.7 % *ee*, which is in good agreement with the experimentally observed 91 % *ee* at 60°C (Figure 6c). To further explain this selectivity, we conducted activation strain analysis (ASA) on both diastereomeric transition states. In this analysis, the TS is partitioned into two fragments: the phenanthrene-9,10-dione fragment and the Rh complex fragment, comprising the remaining portion of the catalytic system (Section17 in SI). ASA reveals that the interaction energy in **TS(E-Fs)** is 8.5 kcal mol^{-1} higher than in **TS(E-F$_R$)** (Figure 6b). Although **TS(E-Fs)** exhibits a 2.3 kcal mol^{-1} higher distortion energy compared to **TS(E-F$_R$)**, the stronger interaction between the fragments in **TS(E-Fs)** compensates for this distortion, resulting in the major product as *S* enantiomer. To further quantify these interactions, quantum theory of atoms in molecules (QTAIM) analysis was done, which revealed stronger noncovalent interactions such as C–H--O in the lower energy **TS(E-Fs)** (Figure 6c).

(a)



(b)

TSs	Distortion Energy (kcal mol^{-1})		Interaction Energy (kcal mol^{-1})
	phenanthrene-9,10-dione	Rh complex	
TS(E-F$_S$)	0.5	1.8	-61.2
TS(E-F$_R$)	0.0	0.0	-52.7

(c)

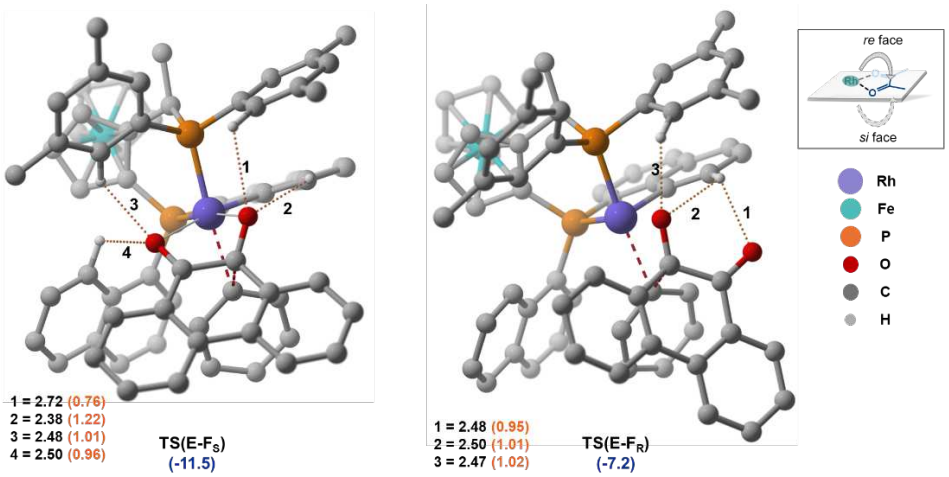


Figure 6. (a) Free energy profile of the arylation reaction catalyzed via $\mathbf{X_1}$ complex. The relative free energies (kcal mol^{-1}) are given at the SMD$_{(toluene:water)}$/B3LYP-D3(BJ)/6-311++G(d,p),SDD(Rh,Fe)//B3LYP-D3(BJ)/6-31G(d,p),SDD(Rh,Fe) level of theory (values shown in black) and PCM$_{(toluene:water)}$/DLPNO-CCSD(T)/def2-TZVP//B3LYP-D3(BJ)/6-31G(d,p),SDD(Rh,Fe) level of theory (values shown in blue). (b) Activation strain analysis for the diastereomeric TSs. (c) The distances are given in Å with the electron densities ($\rho \times 10^{-2}$ au) in parentheses at the bond critical points. Hydrogen atoms are omitted in the CYL view images for clarity, except those involved in noncovalent interactions (NCIs).

Conclusion

In summary, we have redefined the mechanistic basis of dirhodium(II)-catalyzed carbonyl arylation reactions by identifying a mononuclear rhodium species, rather than a dinuclear dirhodium(II) complex, as the true catalytically active entity. Through a comprehensive combination of variable-temperature $^{31}P\{^1H\}$-NMR spectroscopy, high-resolution mass spectrometry, single-crystal X-ray diffraction, additive-controlled experiments, and density functional theory (DFT) calculations, we demonstrate that the dirhodium(II) core undergoes Rh–Rh bond cleavage under the reaction conditions to generate a chiral, orthometalated Rh(III)

complex, **X1**. This complex was further shown to be catalytically competent for carbonyl reaction where it also exhibited higher reactivity and selectivity for phenanthrene-9,10-dione.

More broadly, this work challenges the prevailing assumption that dirhodium(II) species are invariably responsible for catalysis in reactions employing bisphosphines ligand. By unveiling a previously overlooked pathway involving Rh–Rh bond cleavage and orthometalation under catalytically relevant conditions, our findings fundamentally revise the mechanistic picture of dirhodium(II) catalysis. We expect that similar active species can also form in other dirhodium(II) catalyzed reactions with both chiral and achiral phosphines. Additionally, the chiral orthometalated Rh(III)/bisphosphine complex identified herein represents a previously unexplored class of chiral Rh(III) catalysts, providing a new platform for the development of asymmetric transformations beyond carbonyl arylation. We anticipate that these insights will inform the rational design of future rhodium-based catalytic systems and inspire renewed mechanistic scrutiny of dinuclear metal catalysts in asymmetric synthesis.

Data Availability

All the associated data is available in the Supporting Information. CCDC **2535072** contains the supplementary crystallographic data for this paper. This data can be obtained free of charge via www.ccdc.cam.ac.uk/data_request/cif, or by email-ing data_request@ccdc.cam.ac.uk, or by contacting The Cam-bridge Crystallographic Data Centre, 12 Union Road, Cambridge CB2 1EZ, UK; fax: +44 1223 336033.

Supporting Information

All experimental procedures, computational details, and structural data in CIF format

Author Contributions

G. J. and S. R. designed the experiments. S. R. carried out the experiments and computational calculations. A. M. and D. S. carried out the SCXRD experiments. S. R., D. S., P. D. and A. M. and G. J. analyzed the results. S. R. and G. J. wrote the manuscript with inputs from all authors. All authors reviewed and approved the manuscript.

Acknowledgement

G. J. acknowledges IISc, Bangalore for infrastructure and Supercomputing Education and Research Centre (SERC), IISc for computing time. S. R., D. S. & P. D. thanks the Ministry of Education, Government of India, for the doctoral fellowship through PMRF (Prime Minister's Research Fellowship). We appreciate the help of the Central X-ray Facility, IISc Bangalore for their valuable support for Single Crystal XRD measurements. High-resolution mass spectra (HR-MS) were recorded on equipment procured under the Department of Science and Technology (DST)-FIST grant [Grant No. SR/FST/CS II-040/2015]. We are grateful to Prof. Balaji Rao Jagirdar (IPC, IISc) and Mr. Selvakumar S. for helpful discussions. We thank INF facility at IISc and Mr. Suraj Halder (SSCU, IISc) for carrying out ^{35}Cl-NMR.

References

1. Hrdina, R. Dirhodium(II,II) paddlewheel complexes. *Eur. J. Inorg. Chem.* **2021**, 501–528 (2021).
2. Doyle, M. P., Duffy, R., Ratnikov, M. & Zhou, L. Catalytic carbene insertion into C-H bonds. *Chem. Rev.* **110**, 704–724 (2010).
3. Davies, H. M. L. & Beckwith, R. E. J. Catalytic enantioselective C-H activation by means of metal-carbenoid-induced C-H insertion. *Chem. Rev.* **103**, 2861–2904 (2003).
4. Bulugahapitiya, P., Landais, Y., Parra-Rapado, L., Planchenault, D. & Weber, V. A stereospecific access to allylic systems using rhodium(II)-vinyl carbenoid insertion into Si–H, O–H and N–H bonds. *J. Org. Chem.* **62**, 1630–1641 (1997).
5. Hansen, J. & Davies, H. M. L. High symmetry dirhodium(II) paddlewheel complexes as chiral catalysts. *Coord. Chem. Rev.* **252**, 545–555 (2008).
6. Sambasivan, R. & Ball, Z. T. Metallopeptides for asymmetric dirhodium catalysis. *J. Am. Chem. Soc.* **132**, 9289–9291 (2010).
7. Doyle, M. P. & Forbes, D. C. Recent advances in asymmetric catalytic metal carbene transformations. *Chem. Rev.* **98**, 911–936 (1998).

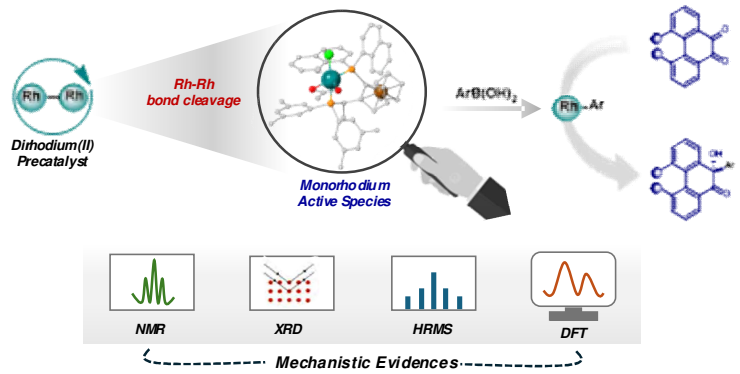
8. Hunter, A. C., Chinthapally, K. & Sharma, I. $Rh_2(esp)_2$: An efficient catalyst for O–H insertion reactions of carboxylic acids into acceptor/acceptor diazo compounds. *Eur. J. Org. Chem.* **2016**, 2260–2263 (2016).
9. Boyar, E. B. & Robinson, S. D. Rhodium(II) carboxylates. *Coord. Chem. Rev.* **50**, 109–208 (1983).
10. Zhu, S.-F. & Zhou, Q.-L. Transition-metal-catalyzed enantioselective heteroatom–hydrogen bond insertion reactions. *Acc. Chem. Res.* **45**, 1365–1377 (2012).
11. Xu, X., Wang, X., Liu, Y. & Doyle, M. P. Enantioselective carbonyl–ene reactions catalyzed by chiral cationic dirhodium(II,III) carboxamidates. *J. Org. Chem.* **79**, 12185–12190 (2014).
12. Wu, R., Xu, Z., Zhu, D. & Zhu, S. Dirhodium-catalyzed asymmetric transformations of alkynes via carbene intermediates. *Acc. Chem. Res.* **58**, 799–811 (2025).
13. Zhang, Y., Yao, Y., He, L., Liu, Y. & Shi, L. Rhodium(II)/chiral phosphoric acid-cocatalyzed enantioselective O–H bond insertion of α-diazo esters. *Adv. Synth. Catal.* **359**, 2754–2761 (2017).
14. Xu, B., Zhu, S.-F., Zhang, Z.-C., Yu, Z.-X., Ma, Y. & Zhou, Q.-L. Highly enantioselective S–H bond insertion cooperatively catalyzed by dirhodium complexes and chiral spiro phosphoric acids. *Chem. Sci.* **5**, 1442–1448 (2014).
15. Ota, K., Lee, S. I., Tang, J. M., Takachi, M., Nakai, H., Morimoto, T., Sakurai, H., Kataoka, K. & Chatani, N. Rh(II)-catalyzed skeletal reorganization of 1,6- and 1,7-enynes through electrophilic activation of alkynes. *J. Am. Chem. Soc.* **131**, 15203–15211 (2009).
16. Davies, H. M. L. & Liao, K. Dirhodium tetracarboxylates as catalysts for selective intermolecular C–H functionalization. *Nat. Rev. Chem.* **3**, 347–360 (2019).
17. Buck, R. T., Coe, D. M., Drysdale, M. J., Ferris, L., Haigh, D., Moody, C. J., Pearson, N. D. & Sanghera, J. B. Asymmetric rhodium carbene insertion into the Si–H bond: Identification of new dirhodium(II) carboxylate catalysts using parallel synthesis techniques. *Tetrahedron: Asymmetry* **14**, 791–816 (2003).
18. Ma, Q., Ma, Y., Liu, X., Duan, W., Qu, B. & Song, C. Planar chiral imidazolium salts based on [2.2]paracyclophane in the asymmetric rhodium-catalyzed 1,2-addition of arylboronic acids to aldehydes. *Tetrahedron: Asymmetry* **21**, 292–298 (2010).
19. Wang, D., Ma, Y., He, F., Duan, W., Zhao, L. & Song, C. Synthesis of planar chiral [2.2]paracyclophanyl imidazo[1,5-α]pyridinium salts for the rhodium-catalyzed asymmetric arylation. *Synth. Commun.* **43**, 810–825 (2013).
20. He, W.-P., Zhou, B.-H., Zhou, Y.-L., Li, X.-R., Fan, L.-M., Shou, H.-W. & Li, J. Synthesis of new benzimidazolium salts and their application in the asymmetric arylation of aldehydes. *Tetrahedron Lett.* **57**, 3152–3155 (2016).
21. Duan, W., Ma, Y., Qu, B., Zhao, L., Chen, J. & Song, C. Synthesis of new alkoxy/sulfonate-substituted carbene precursors derived from [2.2]paracyclophane and their application in the asymmetric arylation of aldehydes. *Tetrahedron: Asymmetry* **23**, 1369–1375 (2012).
22. Trindade, A. F., Gois, P. M. P., Veiros, L. F., André, V., Duarte, M. T., Afonso, C. A. M., Caddick, S. & Cloke, F. G. N. *J. Org. Chem.* **73**, 4076 (2008).
23. Balhara, R., Chatterjee, R. & Jindal, G. Mechanism and stereoselectivity in metal- and enzyme-catalyzed carbene insertion into X–H and C(sp^2)–H bonds. *Chem. Soc. Rev.* **53**, 11004–11044 (2024).
24. Cheng, Q., Tu, H.-F., Zheng, C., Qu, J.-P., Helmchen, G. & You, S.-L. Iridium-catalyzed asymmetric allylic substitution reactions. *Chem. Rev.* **119**, 1855–1969 (2019).

25. Zhang, Y., Zhang, J.-J., Lou, L., Lin, R., Cramer, N., Wang, S.-G. & Chen, Z. Recent advances in Rh(I)-catalyzed enantioselective C–H functionalization. *Chem. Soc. Rev.* **53**, 3457–3484 (2024).
26. Lu, B., Liang, X., Zhang, J., Wang, Z., Peng, Q. & Wang, X. Dirhodium(II)/Xantphos-catalyzed relay carbene insertion and allylic alkylation process: Reaction development and mechanistic insights. *J. Am. Chem. Soc.* **143**, 11799–11810 (2021).
27. Zhang, J., Lu, B., Ge, Z., Wang, L. & Wang, X. Selective construction of all-carbon quaternary centers via relay catalysis of indole C–H functionalization/allylic alkylation. *Org. Lett.* **24**, 8423–8428 (2022).
28. Shi, L., Xue, X., Hong, B., Li, Q. & Gu, Z. Dirhodium(II)/phosphine catalyst with chiral environment at bridging site and its application in enantioselective atropisomer synthesis. *ACS Cent. Sci.* **9**, 748–755 (2023).
29. Zhan, S., Xu, H., Hong, B. & Gu, Z. Quaternary chiral phthalides enabled by dirhodium(II)/phosphine-catalyzed asymmetric carbonyl addition cascade. *Org. Lett.* **26**, 8023–8027 (2024).
30. Guo, W., Zhan, S., Yang, H. & Gu, Z. Confronting the challenge of asymmetric carbonyl addition to sterically bulky isatins: Upgrading dirhodium(II)/biphosphine catalytic system. *Org. Lett.* **25**, 3281–3286 (2023).
31. Zhan, S., Wang, C., Duan, L. & Gu, Z. Chiral benzo[2.2.1] α-hydroxyketones from a dirhodium(II)/bisphosphine-catalyzed desymmetrization addition reaction. *Chem. Sci.* **16**, 19397–19402 (2025).
32. Xu, G., Chen, H. & Wang, X. Enantioselective β-alkenylation of α,β-unsaturated aldehydes via chiral biphosphine ligand-modified dirhodium(II) catalysis. *Sci. China Chem.* **68**, 3138–3146 (2025).
33. Yang, L., Wu, X., Lu, W., Lu, Y. & Zhang, Z. Dirhodium(II)/DPPM-catalyzed 1,2-hydrosilylation of conjugated dienes with tertiary silanes. *Org. Lett.* **26**, 2287–2291 (2024).
34. Lu, W., Zhu, X., Yang, L., Wu, X., Xie, X. & Zhang, Z. Distinct catalytic performance of dirhodium(II) complexes with ortho-metalated DPPP in dehydrosilylation of styrene derivatives with alkoxysilanes. *ACS Catal.* **11**, 10190–10197 (2021).
35. Zhang, C. Bisphospholane Josiphos-type ligands in rhodium asymmetric catalysis. *Chem. Asian J.* **18**, e202300912 (2023).
36. Brüning, F., Nagae, H., Käch, D., Mashima, K. & Togni, A. Asymmetric hydrogenation of aryl perfluoroalkyl ketones catalyzed by rhodium(III) monohydride complexes bearing Josiphos ligands. *Chem. Eur. J.* **25**, 10818–10822 (2019).
37. Chen, H., Yang, W., Zhang, J., Lu, B. & Wang, X. Divergent geminal alkynylation–allylation and acylation–allylation of carbenes: Evolution and roles of two transition-metal catalysts. *J. Am. Chem. Soc.* **146**, 4727–4740 (2024).
38. Telser, J. & Drago, R. S. Solution chemistry of rhodium trifluoroacetate in the presence of phosphorus donors. *Inorg. Chem.* **25**, 2989–2992 (1986).
39. Shi, R., Tan, J., Wang, Z. & Wang, Y. Oxidatively induced selective carbon–carbon bond formation from isolated rhodium(III) complexes. *Chem. Eur. J.* **27**, 14317–14321 (2021).
40. Telser, J. & Drago, R. S. Reactions of rhodium trifluoroacetate with various Lewis bases: Formation of 4:1 complexes with pyridine and tert-butyl isocyanide and bond cleavage with phosphorus donors. *Inorg. Chem.* **23**, 2599–2606 (1984).
41. Frisch, M. J. *et al. Gaussian 16, Revision C.01* (Gaussian, Inc., Wallingford, CT, 2016).

42. Grimme, S., Antony, J., Ehrlich, S. & Krieg, H. A consistent and accurate *ab initio* parametrization of density functional dispersion correction (DFT-D) for the 94 elements H–Pu. *J. Chem. Phys.* **132**, 154104 (2010).
43. Hay, P. J. & Wadt, W. R. *Ab initio* effective core potentials for molecular calculations. Potentials for K to Au including the outermost core orbitals. *J. Chem. Phys.* **82**, 299–310 (1985).
44. Gonzalez, C. & Schlegel, H. B. An improved algorithm for reaction path following. *J. Chem. Phys.* **90**, 2154–2161 (1989).
45. Nicklass, A., Dolg, M., Stoll, H. & Preuss, H. *Ab initio* energy-adjusted pseudopotentials for the noble gases Ne through Xe: Calculation of atomic dipole and quadrupole polarizabilities. *J. Chem. Phys.* **102**, 8942–8952 (1995).
46. Becke, A. D. Density-functional thermochemistry. III. The role of exact exchange. *J. Chem. Phys.* **98**, 5648–5652 (1993).
47. Lee, C., Yang, W. & Parr, R. G. Development of the Colle–Salvetti correlation-energy formula into a functional of the electron density. *Phys. Rev. B* **37**, 785–789 (1988).
48. Dolg, M., Wedig, U., Stoll, H. & Preuss, H. Energy-adjusted *ab initio* pseudopotentials for the first row transition elements. *J. Chem. Phys.* **86**, 866–872 (1987).
49. Fukui, K. The path of chemical reactions—the IRC approach. *Acc. Chem. Res.* **14**, 363–368 (1981).
50. Marenich, A. V., Cramer, C. J. & Truhlar, D. G. Universal solvation model based on solute electron density and on a continuum model of the solvent defined by the bulk dielectric constant and atomic surface tensions. *J. Phys. Chem. B* **113**, 6378–6391 (2009).
51. Chakravarty, A. R., Cotton, F. A., Tocher, D. A. & Tocher, J. H. Structural and electrochemical characterization of the novel ortho-metalated dirhodium(II) compounds $Rh_2(O_2CMe)_2[Ph_2P(C_6H_4)]_2 \cdot 2L$. *Organometallics* **4**, 8–13 (1985).
52. Cotton, F. A., Murillo, C. A., Stiriba, S.-E., Wang, X. & Yu, R. Chiral organometallic triangles with Rh–Rh bonds. 2. Compounds prepared from enantiopure cis-$Rh_2(C_6H_4PPh_2)_2(OAc)_2(HOAc)_2$ and their catalytic potentials. *Inorg. Chem.* **44**, 8223–8233 (2005).
53. Cotton, F. A. & Caulton, K. G. Crystal and molecular structure of bis(triphenylphosphine)tetrakis(dimethylglyoximato)dirhodium. Length of a rhodium(II)-to-rhodium(II) single bond. *J. Am. Chem. Soc.* **93**, 1914–1918 (1971).
54. Cotton, F. A. & Norman, J. G. Jr. Crystal and molecular structure of chlorobis(dimethylglyoximato)triphenylphosphinerhodium(III). *J. Am. Chem. Soc.* **93**, 80–84 (1971).
55. Estevan, F., Herbst, K., Lahuerta, P., Barberis, M. & Pérez-Prieto, J. Chiral dirhodium(II) catalysts with orthometalated aryl phosphine ligands: Synthesis and application for enantioselective C–H insertion of α-diazo ketones. *Organometallics* **20**, 950–957 (2001).
56. Lloret, J., Estevan, F., Lahuerta, P., Hirva, P., Pérez-Prieto, J. & Sanaú, M. Dirhodium(II) compounds with bridging thienylphosphines: Studies on reversible P,C/P,S coordination. *Chem. Eur. J.* **15**, 7706–7716 (2009).
57. Lahuerta, P., Paya, J., Pellinghelli, M. A. & Tiripicchio, A. Fast ortho-metalation reactions in binuclear dirhodium compounds. Syntheses and molecular structures of a monometalated compound and two doubly metalated compounds with head-to-head configurations. *Inorg. Chem.* **31**, 1224–1232 (1992).

58. Estevan, F., Lahuerta, P., Pérez-Prieto, J., Sanaú, M., Stiriba, S.-E. & Ubeda, M. A. Ligand effects on the chemoselectivity of ortho-metalated rhodium(II)-catalyzed α-diazo ketone transformations. *Organometallics* **16**, 880–886 (1997).
59. Barberis, M., Estevan, F., Lahuerta, P., Pérez-Prieto, J. & Sanaú, M. New dinuclear catalysts $Rh_2(N–O)_2[(C_6H_4)P(C_6H_5)_2]_2$ with imidate ligands: Synthesis and isomerization from head-to-tail to head-to-head configuration of the imidate ligands. *Inorg. Chem.* **40**, 4226–4229 (2001).
60. Lahuerta, P., Paya, J., Solans, X. & Ubeda, M. A. Ortho-metalation reactions in binuclear dirhodium compounds. Molecular structure and reactivity of a monometalated compound with the phosphine $P(o\text{-}ClC_6H_4)(C_6H_5)_2$. *Inorg. Chem.* **31**, 385–391 (1992).
61. Cotton, F. A., Barcelo, F., Lahuerta, P., Llusar, R., Paya, J. & Ubeda, M. A. Ortho-metalation reactions in binuclear dirhodium compounds. Synthesis and molecular structure of an unsymmetrical Rh_2^{4+} compound with two different ortho-metalated phosphines. *Inorg. Chem.* **27**, 1010–1013 (1988).
62. Barcelo, F., Cotton, F. A., Lahuerta, P., Llusar, R., Sanau, M., Schwotzer, W. & Ubeda, M. A. Synthesis and structure of the ortho-metalated dirhodium(II) compound $Rh_2(O_2CCH_3)_3[(C_6H_4)P(C_6H_5)(C_6F_4Br)]\cdot P(C_6H_5)_2(C_6F_4Br)$. *Organometallics* **5**, 808–811 (1986).
63. Taber, D. F., Malcolm, S. C., Bieger, K., Lahuerta, P., Sanaú, M., Stiriba, S.-E., Pérez-Prieto, J. & Monge, M. A. Synthesis, structure, and reactivity of the first enantiomerically pure ortho-metalated rhodium(II) dimer. *J. Am. Chem. Soc.* **121**, 860–861 (1999).
64. Tresoldi, G., De Munno, G., Nicolò, F., Lo Schiavo, S. & Piraino, P. Synthesis and NMR investigation of dirhodium(II) formamidinate complexes containing bidentate phosphorus donors. X-ray crystal structure of the ortho-metalated complex $Rh_2(Form)(\mu\text{-}O_2CCF_3)(C_6H_4)(C_6H_5)P(CH_2)_2P(C_6H_5)_2$(p-toluidine). *Inorg. Chem.* **35**, 1377–1381 (1996).
65. Fu, L., Li, S., Cai, Z., Ding, Y., Guo, X.-Q., Zhou, L.-P., Yuan, D., Sun, Q.-F. & Li, G. Ligand-enabled site-selectivity in a versatile rhodium(II)-catalysed aryl C–H carboxylation with CO_2. *Nat. Catal.* **1**, 469–478 (2018).
66. Van Dijk, L., Ardkhean, R., Sidera, M., Karabiyikoglu, S., Sari, Ö., Claridge, T. D. W., Lloyd-Jones, G. C., Paton, R. S. & Fletcher, S. P. Mechanistic investigation of Rh(I)-catalysed asymmetric Suzuki–Miyaura coupling with racemic allyl halides. *Nat. Catal.* **4**, 284–292 (2021).

TOC Graphics



Supplementary Files

This is a list of supplementary files associated with this preprint. Click to download.

- SI2062026.docx